The Challenge of Lower Temperature Soldering for Large Ball-Grid Array (BGA) Board-Level Assembly – Phase 1. Processing

Hongwen Zhang, Ph.D., Francis Mutuku, Ph.D., Huaguang Wang, Ph.D.
Indium Corporation
Clinton, New York, USA

ABSTRACT

Low temperature soldering (reflow peak temperature at 200°C and below) has been considered as one of the effective ways to reduce the processing defects caused by warpage of large BGA assembly. Most of the large BGAs are still surfaced with SnAgCu (SAC) and/or modified SAC balls, whose melting temperature ranges from 210°C to 220°C. Although BGA warpage can be reduced under low reflow temperature, the limited solder paste volume, because SnAgCu ball will not melt but dissolve during reflow, may still be insufficient to compensate for the mitigated warpage, possibly resulting in forming the defective joints, including non-contact, head-in-pillow and non-wet-open etc. Adding more paste would reduce the possibility of forming afore-mentioned defective joints but bring in the risk of joint bridging. Increasing the reflow peak temperature may enlarge the component warpage but allow more molten solder volume during soldering, which may compensate for the warpage displacement and help the joint formation as well. Hot-tearing from using low temperature solder is another concern related to the overlap of component warpage inversion temperature and solder solidification temperature. Thus, optimization of both paste volume and reflow temperature, as well as selection of the appropriate solder alloy are critical to succeed.

The current article has systematically, in the first time, investigated the joint formation through the selection of (1) solder alloys of different melting temperature (138°C for BiSnAg eutectic, 205°C for DFLT-1 and 196°C for DFLT-2), (2) paste to ball volume ratio (PBVR of 0.13, 0.25 and 0.5), and (3) reflow profiles (low temperature reflow of 185 and 200°C peak, mid temperature reflow of 210 and 220°C, and traditional SAC reflow of 240°C peak) with a 40x40mm^2 PBGA928 component (max concave warpage of -11mil at 100°C and max convex warpage of 34mil at 250°C with inversion temperature of 140°C).

Defective joints are always seen under low temperature soldering for all three pastes regardless of PBVR. Increasing reflow temperature to above 200°C improved the joint shape and greatly reduced the defects. Under P220 and PBVR of 0.13, all three pastes have achieved the optimal joints without "fatal" defects. DOE analysis had confirmed the reflow peak is the most impact factor to form the optimal joint, followed by PBVR and alloy selection. SAC/BiSnAg joints were dominated by hot-tearing under low temperature reflows, whose wide pasty range, overlapped with the component inversion temperature of 140°C, is attributed to the higher occurrence. SAC/DFLT and SAC/DFLT-2 had much narrower pasty range and always solidified above the inversion temperature, showing much less hot tearing. The investigation of the joint reliability performance is still ongoing and will be presented in Phase II.

Key words: Lead-free Solder, Low-temperature Soldering, Ball-grid array, Reflow, Warpage, Hot-tearing, Head-in-pillow, Assembly.

INTRODUCTION

The development of heterogeneous integration assemblies (HIA) that combine multiple chips of varying types into a single package mitigated the limitation of the lithographic scaling in high-density semiconductor integrated circuits [1, 2, 3]. This compartmentalization serves as an alternative way to provide the improved computing capability required for the data-intensive future [4, 5]. The increasing ball grid array (BGA) package size associated with the HIA architecture for high performance computing leads to the challenges on the design to qualification and the mass-production readiness etc., because of the significant package warpage of the design [6, 7, 8]. The warpage of the packages, especially the dynamic warpage related to temperature variation, also leads to challenges in the board-level assembly [9]. To reduce the impact of the package warpage on the PCB assembly, low temperature soldering has commonly been proposed and attempted [10, 11, 12, 13].

Most of the BGA components are still surfaced with SAC and SAC-based solder balls, whose melting temperature is above 210°C. Under low temperature reflow (reflow peak temperature of 200°C and below), SAC and SAC-based solder balls are not melting but dissolving into the molten low temperature solders. It is still risky of forming defective joints because of the insufficient molten solder volume to compensate for the mitigated warpage under low temperature soldering. The malformed joints, characterized by various defects including head-in-pillow (HIP), non-contact open (NCO), non-wetting open (NWO), necking and/or hot-tearing, have been seen under low temperature soldering [10, 14, 15]. Increasing paste volume will alleviate the afore-mentioned defects while bringing another risk of joint bridging. Raising reflow temperature to have more solder ball alloy dissolved or even fully molten during soldering would assist forming the optimal joints if the change of component warpage is still able to be compensated. Hot tearing was reported under low temperature soldering and rationalized to the overlap of component inversion temperature and solder solidification [16]. Thus, alloy selection relative to the component dynamic warpage inversion must be considered as well. However, there is no systemic investigation on the joint formation for a large BGA package with significant dynamic warpage.

The current study investigated, for the first time, the formation of the desirable joint for a large plastic BGA (PBGA928 with SAC305 Balls) package with known dynamic warpage, from three aspects, (1) the selection of low melting solder alloys with full melting temperature from 138°C for eutectic BiSnAg, 196°C for DFLT-2 and upto 205°C for DFLT; (2) the reflow profiles with varied peak temperature regime from low temperature of 185 and 200°C, mid temperature of 210 and 220°C, and upto 240°C of traditional SAC305 profile; and (3) the PBVRs (paste-to-ball-volume-ratio) of 0.13, 0.25 to 0.5. DOE analysis on the testing data is followed to rationalize the impact of each aspect.

EXPERIMENTAL METHODOLOGY

Solder Materials

Three solders with different metallurgical designs and associated melting temperatures were selected. Bismuth-tin-based eutectic solder alloy (BiSnAg) has a melting point of 138°C. Two Bi-free In-containing lower temperature solders have been selected, including a) DFLT with the melting temperature range of 189 to 205°C and b) DFLT-2 with the melting temperature range of 180 to 196°C. Table 1 has summarized the composition and the melting range of three solder materials in the study. The melting behavior difference is expected to be present and impact joint formation.

Table 1: The Composition and the Melting Temperature of the Selected Solders.

	Bi	Sn	In	Ag	Cu	Ts(°C)	Tl(°C)
BiSnAg	57	42	-	1		138	138
DFLT	-	84.4	12.5	2.9	0.2	189	205
DFLT-2	-	78.8	16.9	3.5	0.7	180	196

Testing Vehicles

Table 2 shows the blueprint and the parameters of PBGA928 used in the current study. Along the outmost row or column, there are 37 total joints. BGA ball is SAC305 with the diameter of 0.63mm and the pitch size is 1mm.

Table 2: The Blueprint of PBGA928 (SAC305 Ball).

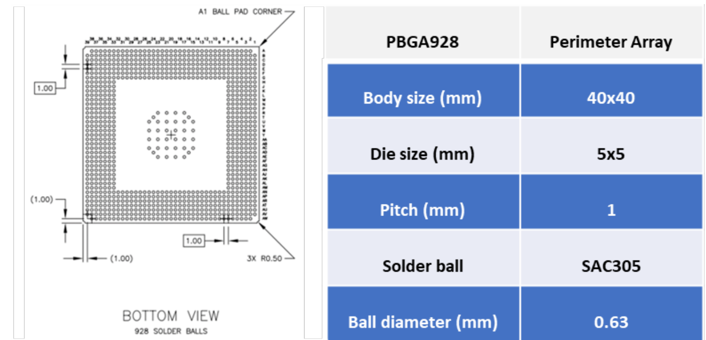

PBGA928	Perimeter Array
Body size (mm)	40x40
Die size (mm)	5x5
Pitch (mm)	1
Solder ball	SAC305
Ball diameter (mm)	0.63

The dynamic warpage of PBGA928, in Figure 1, has been measured with Shadow Moiré method [17]. There is a slight concave warpage of PBGA928 at room temperature. The largest concave warpage (-10mils) was seen around 100°C. The concave warpage will gradually decrease to zero when the temperature rises to around 140°C, the warpage inversion temperature. Beyond 140°C, the convex warpage was then dominated with a maximum of around 34mils at 250°C.

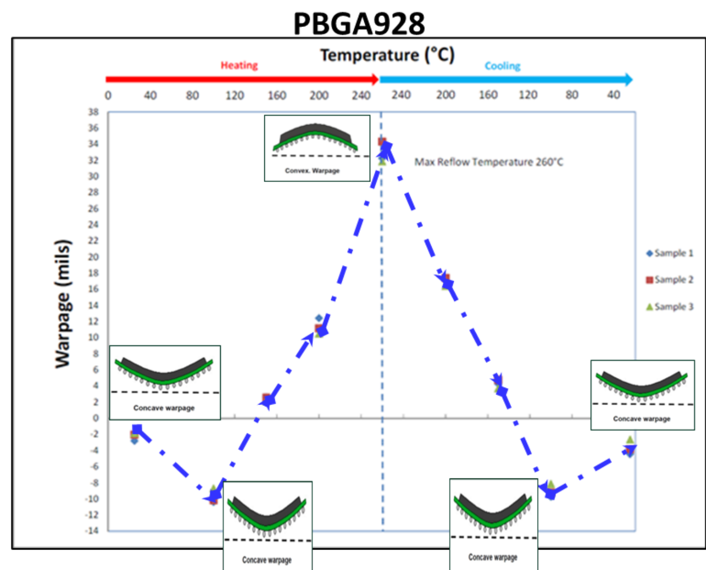

Figure 1: The dynamic warpage of PBGA928

Table 3 provides the PCB design and the parameters for the assembly.

Table 3: PCB Design and Reflowed Assembly.

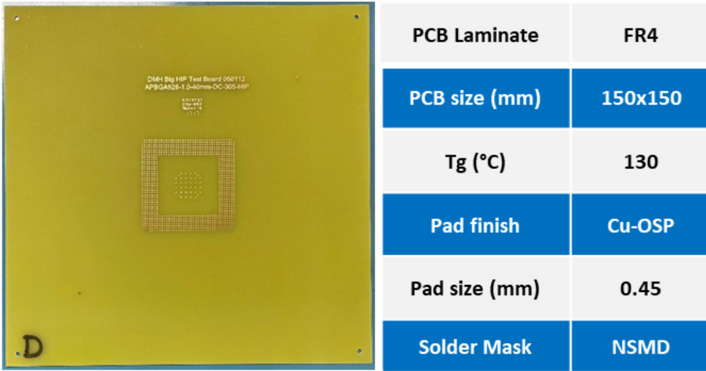

PCB Laminate	FR4
PCB size (mm)	150x150
Tg (°C)	130
Pad finish	Cu-OSP
Pad size (mm)	0.45
Solder Mask	NSMD

Reflow Profiles

Various reflow profiles, including P185, P200, P210, P220 and P240 with peak temperatures of around 185.2°C, 203.8°C, 213.1°C, 222.7°C and 236.7°C respectively, have been used. Figure 2 shows the reflow profiles.

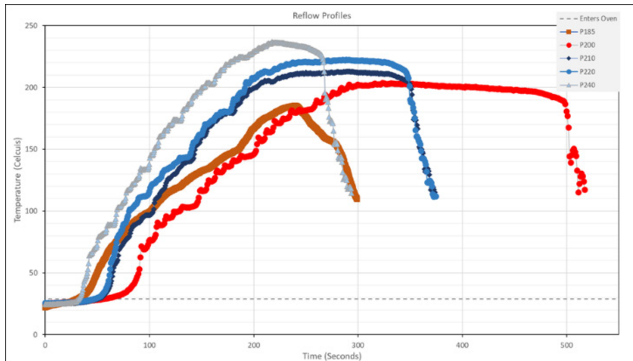

Figure 2: Reflow Profiles.

P220 profiles, in which P185 profile was commonly used for BiSn-based LTS assembly build. DFLT had been reflowed with P200, P210, P220 and P240 profiles while DFLT-2 were reflowed with P200, P210 and P220 profiles. Table 4 has summarized the actual reflow peak temperature and the time above liquidus temperature (TAL) for each paste.

Table 4: Summary of Reflow Profiles.

Profile #	Peak Temperature (°C)	TAL (s) for BiSnAg	TAL(s) for DFLT	TAL(s) for DFLT-2
P185	185.2	117	-	-
P200	203.8	290	145	200
P210	213.1	-	124	157
P220	222.7	241.8	151	168
P240	236.7	-	65	-

Stencil Design

Three stencils have been designed to maintain the paste-to-ball volume ratios (PBVR) around 0.13, 0.25 and 0.5, which is shown in Table 5. To enhance the warpage impact, the stencil was designed to skip the center pattern aperture, only keeping the perimeter aperture open, where no paste was to be printed onto the PCB in the center area. It is designed to see whether the perimeter joints handle well the displacement caused by warpage without the assistance of center joints to hold the package from convex warpage under soldering.

Table 5: The Stencil Design for Paste-to-Ball Volume Ratio (PBVR).

Stencil #	Thickness (mm)	Circular Aperture (mm)	PBVR	Aspect Ratio	Area Ratio
#1	0.1	0.46	0.13	4.6	1.15
#2	0.125	0.58	0.25	4.6	1.16
#3	0.175	0.69	0.5	3.9	0.98

Testing Matrix

BiSnAg, holding the lowest melting temperature among all three pastes, was reflowed under P185 and P200 profiles with PBVRs of 0.13, 0.25 and 0.5. BiSnAg has also been reflowed under P220 profile with PBVR of 0.13 and 0.5 respectively. DFLT, with the highest melting temperature among all three pastes, was reflowed under P200 and P210 with PBVRs of 0.13, 0.25 and 0.5, while under P220 and P240 with only a PBVR of 0.13. DFLT-2 had been reflowed under P200 and P210 profiles with PBVRs of 0.13, 0.25 and 0.5 while under P220 with only a PBVR of 0.13. Table 6 displays the testing matrix. For each condition in the matrix, two assemblies have been built.

Table 6: Testing Matrix for Assembly Built.

	PBVR	Reflow				
		P185	P200	P210	P220	P240
BiSnAg	0.13	x	x		x	
	0.25	x	x			
	0.5	x	x		x	
DFLT	0.13		x	x	x	x
	0.25		x	x		
	0.5		x	x		
DFLT-2	0.13		x	x	x	
	0.25		x	x		
	0.5		x	x		

X-ray inspection and Metallographic Observation

After reflow, X-ray inspection was used to check the joint formation from each assembly. Afterwards one of the assemblies from each condition was selected for cross-section and metallographic observation. Figure 3 shows the example image of the reflowed assembly, and the cross-section cut along line A, the outmost row of the assembly. Cross-section images would be taken by optical microscopy and scanning electron microscopy (SEM). The other assembly was kept for TCT.

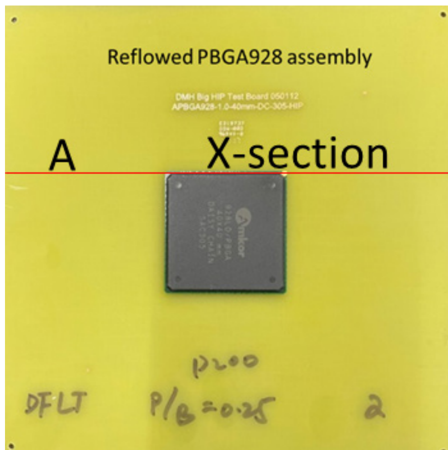

Figure 3: Example Image of the Reflowed Assembly with Indicated Cross Section for Microscopy.

RESULTS

BiSnAg Eutectic

Under P185 profile and a PBVR of 0.13, BiSnAg formed the defected joints almost all over the board. Both necking and non-contact open joints are shown in X-ray images of Figure 4. The left and right images in Figure 3 are from the diagonal corners of the same assembly. The tilt of BGA928 relative to PCB is noticeable as the formation of its necking joints are concentrated toward one corner (right image of Figure 3) while almost all the joints are open at the opposite corner. The cross-section metallographic images of the selected 4 out of 37 joints (#1, #16, #24, and #37) from the outmost row of the same assembly in Figure 5 had confirmed the defects of non-contact open joint (Joint #1), the open necking (Joint #16), the necking (#24 and #37) and the tilt (different joint heights from left to right). The non-contact open joints of one corner would be caused by the tilt, which might be the result of the perimeter aperture design of the stencil, the wetting imbalance of the large BGA, and the insufficient solder paste. The necking joints indicated the insufficient molten solder to handle the warpage during reflow.

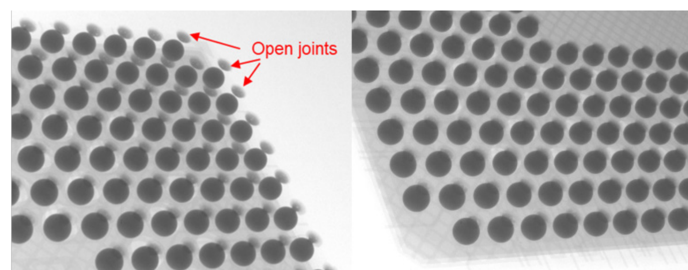

Figure 4: Joints Formed at Diagonal Corners of the BiAgSn, P185, PBVR=0.13.

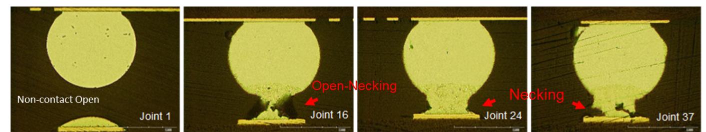

Figure 5: Joints Along Raw of BiSnAg, P185, PBVR = 0.13.

Under P185 and a PBVR of 0.25, the non-contact open joints for BiSnAg were not clearly observable while the necking joints were still clustered at one corner in Figure 6 (left). The opposite corner had formed a better joint shape. No open joint was observed, but the necking (Joint #16 and #24), the half-necking joints (Joint #1) and even the partial-open-necking (joint #37) were clearly visible Figure 6. The necking is relieved in the middle joints, but still not acceptable. Interfacial hot-tearing delamination and interfacial voids between solder and PCB pad were observed as well in Figure 7. Also, it is noticed that corner joints are taller than middle ones as shown in Figure 7, indicating the concave warpage of the assembly after reflow.

	PBVR	Reflow				
		P185	P200	P210	P220	P240
BiSnAg	0.13	x	x		x	
	0.25	x	x			
	0.5	x	x		x	
DFLT	0.13		x	x	x	x
	0.25		x	x		
	0.5		x	x		
DFLT-2	0.13		x	x	x	
	0.25		x	x		
	0.5		x	x		

Figure 6: Joints Formed at the Diagonal Corners of the SnAg, P185, PBVR = 0.25.

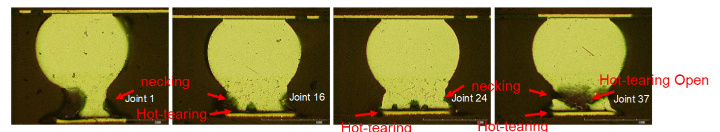

Figure 7: Joints Along Raw of BiSnAg, P185, PBVR=0.25.

With a PBVR of 0.5 under the P185 profile, BiSnAg had still presented the necking joints on one corner as shown in Figure 8 (left) and the elongated-oval joints together with a few necking joints on the opposite corner in Figure 8 (right). Figure 9 had confirmed the hot-tearing along the neck of the corner joints (Joint 1 and Joint 27) and the elongated oval one in the middle (Joint16 and Joint 24). It may indicate that the increased low temperature paste volume is still not able to handle the warpage. Interfacial delamination along the joint corner was not clearly seen. Still, it is seen that corner joints are taller than middle ones (concave warpage) as in Figure 9.

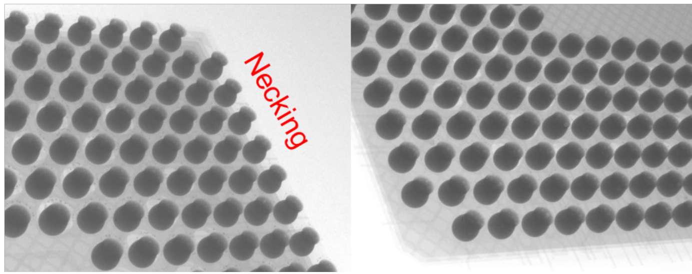

Figure 8: Joints Formed at the Diagonal Corners of the BiSnAg, P185, PBVR = 0.5.

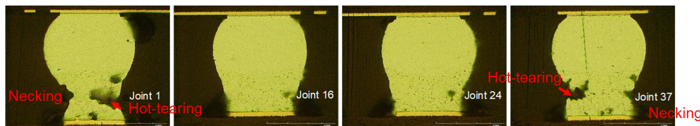

Figure 9. Joints Along Raw of BiSnAg, P185, PBVR = 0.5.

Switching to P200 profile, BiSnAg had formed most of the oval joints even with a PBVR of 0.13 while voids were discovered in almost all joints shown in Figure 10. However, there is no significant difference in joint shape formed in the opposing corners. The oval joints were observed along the whole row in Figure 11. The middle joints (#16 and #24) were well-formed in the oval shape even though the voids (both round and irregular shape) were present. The round void resulted from in-trapped volatile bubbles and the irregular voids might be caused in turn by shrinkage voids. The corner joints have presented the shrinkage voids and the hot-tearing delamination from PCB pads together with the slightly elongated shape. Again, one of the corner joint (Joint 1) is clearly taller than middle joints (Joint 16 and 24) and another corner joint (Joint37) is just slightly taller than middle ones, maintaining concave type warpage as in Figure 11.

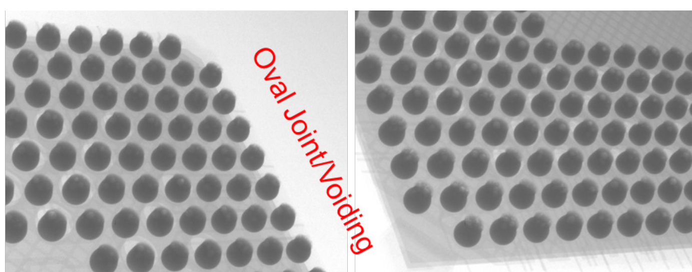

Figure 10: Joints Formed at the Diagonal Corners of the BiSnAg, P200, PBVR = 0.13.

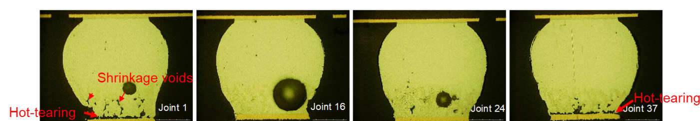

Figure 11: Joints Along Raw of BiSnAg, P200, PBVR = 0.13.

Increasing the PBVR to 0.25 under the same P200 profile, the joints were oval-shaped in Figure 12. The corner joints (Joint #1 and Joint #37) exhibited slightly elongated shape, bubble voiding, shrinkage voiding, and the hot-tearing delamination (Figure 13) while the middle joints (Joint #16 and Joint #24) are acceptable in morphology. Joint #37 also presented necking between the SAC ball and PCB pad. The oval joints with some noticed voids were observed in the middle of the row. Joint 1 at the left corner is evidently taller than middle ones while Joint 37 at the right corner is barely as tall as middle ones in Figure 13.

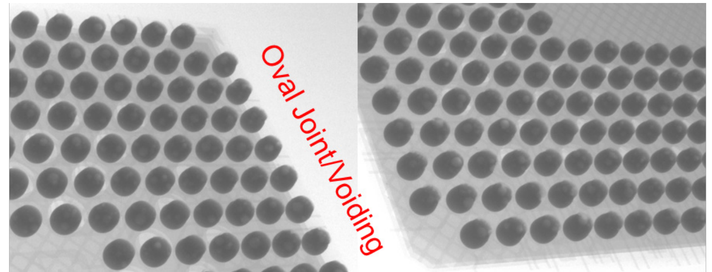

Figure 12: Joints Formed at Diagonal Corners of the BiSnAg, P200, PBVR = 0.25.

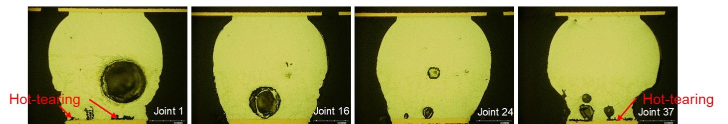

Figure 13: Joints Along Raw of BiSnAg, P200, PBVR = 0.25.

Increasing the PBVR to 0.5 under P200 reflow, most of the joints were still in the oval shape but were prone to spherical form as shown in Figure 14. Indeed, the spherical joints were observed from the middle joints although the oval shape was still present in Figure 15. However, the hot-tearing delamination, shrinkage voids, and bubble voids were present in all four selected joints. Corner joints are almost the same height as middle ones (flat or near-flat) in Figure 15.

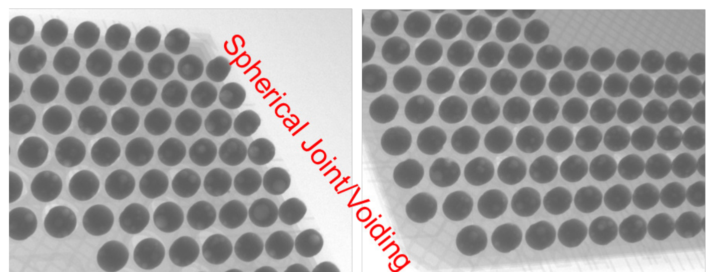

Figure 14: Joints Formed at Diagonal Corners BiSnAg, P200, PBVR = 0.5.

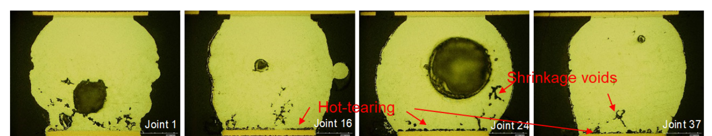

Figure 15: Joints Along Raw of BiSnAg, P200, PBVR = 0.5.

After the attempts with six processing combinations (two reflow profiles and three PBVRs), there were no acceptable morphology formed for SAC/BiSnAg joints using the profiles of 200°C peak and below. It was out of the expectation to see the malformation of the SAC/BiSnAg joint even using P2B ratio of 0.5 and the 200°C peak temperature profile. All the shrinkage voids and the hot-tearing were located at PCB side, which were inside the mixing zone dominated by BiSnAg and partially dissolved SAC305.

Reflow with the peak temperature of 220°C was then tried, which would allow SAC305 melt and merge with BiSnAg low melting solder. The drum shape joints under P220 and PBVR of 0.13 were confirmed from X-ray in Figure 16 though voids were still presented. These joints were in good drum shape without any noticed hot-tearing and shrinkage voids in Figure 17. Different from lower temperature reflow (P185 and P200), middle joints (Joint 16 and 24) are slightly taller than corner ones, indicating the convex warpage instead, as shown in Figure 17.

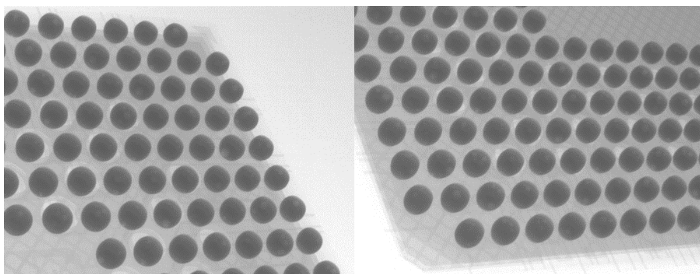

Figure 16: Joints Formed at Diagonal Corners BiSnAg, P220, PBVR = 0.13.

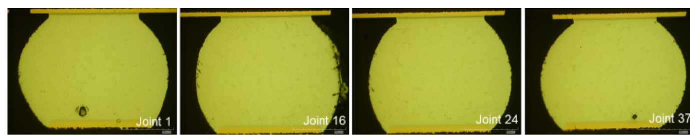

Figure 17: Joints Along Raw of BiSnAg, P220, PBVR = 0.13.

Raising PBVR to 0.5 from 0.13 under the same P220 reflow, joints had formed well in drum shape from X-ray images in Figure 18. Cross-section images in Figure 19 confirmed the drum shape joints, more likely the pear shape. The voids are seen at top of the joints, right beneath the package pads, indicating the full melt of the joints in reflow. Corner joints are taller than middle ones, indicating the concave warpage.

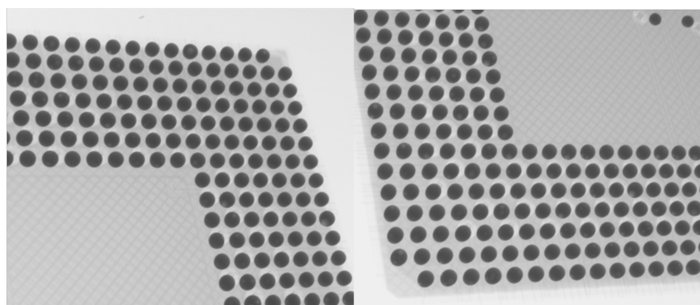

Figure 18: Joints Formed at Diagonal Corners BiSnAg, P220, PBVR = 0.5.

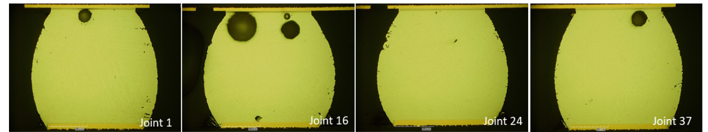

Figure 19: Joints Along Raw of BiSnAg, P220, PBVR = 0.5.

DFLT and DFLT-2

Under P200 profile and PTB volume ratio of 0.13, both DFLT (with a melting temperature from 189 to 205°C) and DFLT-2 (the melting temperature from 180 to 196°C, around 9°C lower than DFLT) demonstrated pronounced necking joints as shown in Figure 20, even though it is noted that DFLT-2 could be seen visually to improve the joint shape. The tilt and open joints were not noticed for either DFLT or DFLT-2. DFLT exhibited severe necking joints, dominating the entire cross-section row of optical images in Figure 21. The corner joints (Joint #1 and Joint #37) of DFLT even had hot-tearing delamination on PCB surface. Joint #2 happened to present the HIP defect, which had also been labeled in Figure 21 (left). Although slightly better than DFLT, DFLT-2, with the lower melting temperature compared to DFLT, still had the necking from all selected joints in Figure 22. Joint #1 even presented both severe necking and hot-tearing delamination. Middle joints are slightly taller than corner ones both DFLT and DFLT-2, indicating the convex warpage as in Figure 21 and 22.

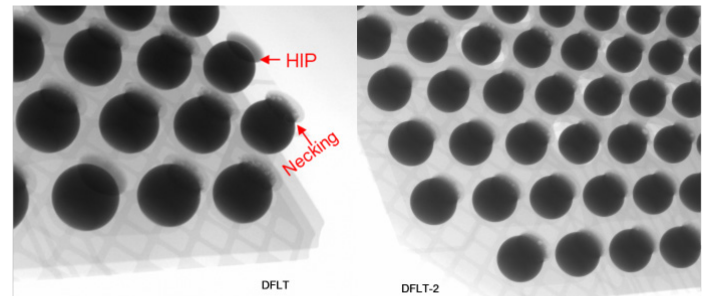

Figure 20: Left: DFLT, P200, PBVR = 0.13; Right: DFLT-2, P200, PBVR = 0.13.

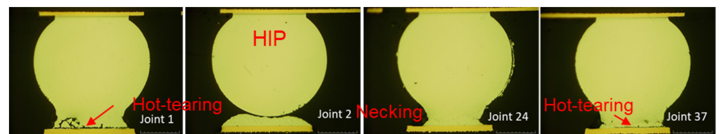

Figure 21: DFLT, P200 Joints, PBVR = 0.13.

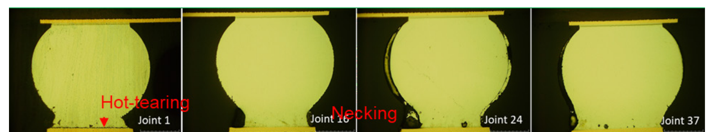

Figure 22: DFLT-2, P200 Joints, PBVR = 0.13.

Increasing PBVR from 0.13 to 0.25 while keeping P200 reflow, necking was still seen for both DFLT and DFLT-2 from the X-ray images in Figure 23. Cross-section images in Figure 24 and 25

confirmed necking especially at the corner joints (Joint 1 and Joint 34) for both alloys. DFLT-2 even had hot-tearing between solder and PCB pad at both corner joints while DFLT did not. Joint height was not significantly different for both alloys (near-flat assembly) from Figure 24 and 25.

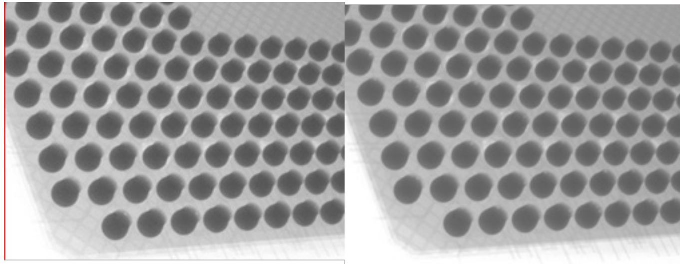

Figure 23: Left: DFLT, P200, PBVR = 0.25; Right: DFLT-2, P200, PBVR = 0.25.

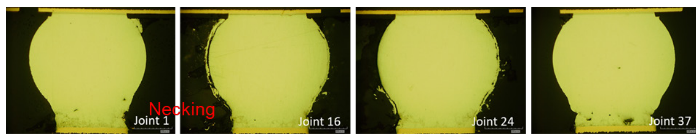

Figure 24: DFLT, P200 Joints, PBVR = 0.25.

Figure 25: DFLT-2, P200 Joints, PBVR = 0.25.

Further increasing PBVR to 0.5, necking was not clearly identified from X-ray images in Figure 26, while the joints were elongated. The elongated joint shape had been verified by cross-sections images for both DFLT and DFLT-2 as seen in Figures 27 and 28. Slightly hot-tearing opening between solder and PCB pad is seen in one corner joint (Joint 1) of DFLT2 while not present in all DFLT joints. Corner joints seem slightly taller than middle ones, especially for DFLT-2 in Figure 28, implying the concave warpage, while near-flat assembly was seen for DFLT in Figure 27.

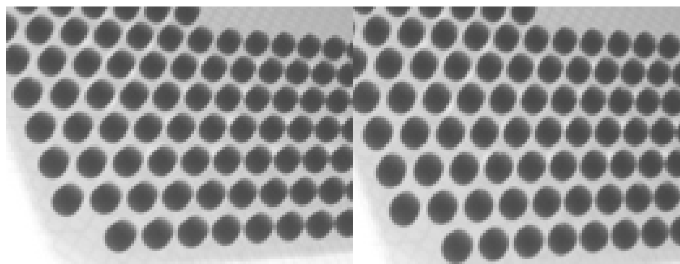

Figure 26: Left: DFLT, P200, PBVR = 0.5; Right: DFLT-2, P200, PBVR = 0.5.

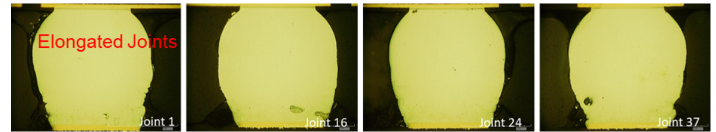

Figure 27: DFLT, P200 Joints, PBVR = 0.5.

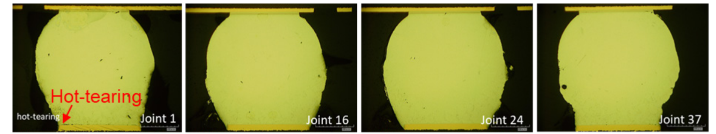

Figure 28: DFLT-2, P200 Joints, PBVR = 0.5.

Using hotter profile of P210 but maintaining the PBVR of 0.13, the joint shape for both DFLT and DFLT-2 tended to be oval or even spherical in shape (Figure 29). The corner joints of both DFLT and DFLT-2 presented the desired drum shape while the middle joints along the same row were still the oval shape with slight necking on the PCB side in Figure 30 and 31. DFLT-2 had slightly reduced necking compared DFLT. No hot-tearing delamination or shrinkage voids occurred in any of the joints in the whole row. Also, it was seen that the middle joints were visually taller than the corner joints for both DFLT and DFLT-2.

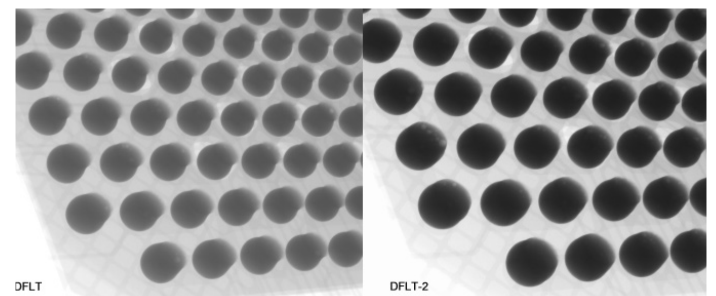

Figure 29: Left: DFLT, P210, PBVR = 0.13; Right: DFLT-2, P210, PBVR = 0.13.

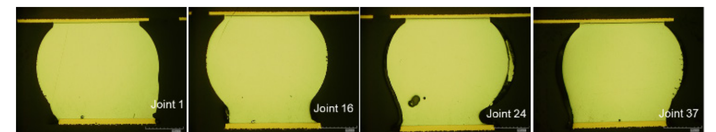

Figure 30: DFLT, P210, PBVR = 0.13. Left: the Corner Joint (C); Right: the Middle Joint (M).

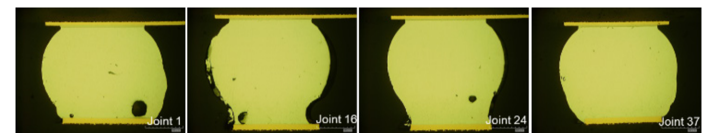

Figure 31: DFLT-2, P210, PBVR = 0.13. Left: the Corner Joint (C); Right, the Middle Joint (M).

Raising the PBVR to 0.25 under the same P210 profile, the joints exhibited the desired, near-spherical shape from X-ray images of Figure 32. The corner joints are more spherical shape while the middle joints are taller, indicating a convex warpage of the assembly,

in the oval shape for both DFLT and DFLT-2 in Figures 33 and 34. No hot-tearing and other defects were seen from all the joint along the outmost row except a couple of small voids close to PCB pad.

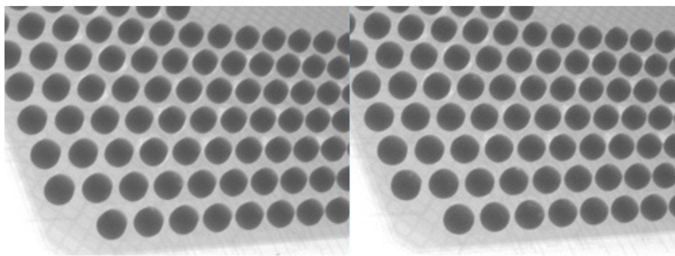

Figure 32: Left: DFLT, P210, PBVR = 0.25; Right: DFLT-2, P210, PBVR = 0.25.

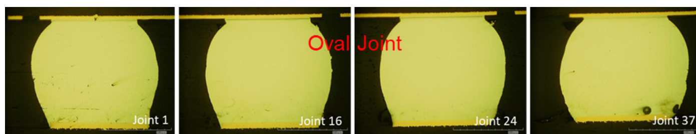

Figure 33: DFLT, P210 Joints, PBVR = 0.25.

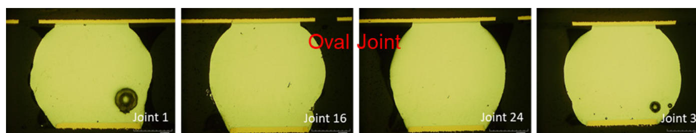

Figure 34: DFLT-2, P210 Joints, PBVR = 0.25.

Increasing PBVR to 0.5 while using P210 profile, the joints were likely in the spherical shape as shown in X-ray images of Figure 35 and the cross-section images in Figure 36 and 37. All the joints for both DFLT and DFLT-2 were healthy without any fatal defects like hot-tearing, HIP, NOW, NCO etc. or even necking. The middle joints are taller than the corner ones for both alloys, keeping convex warpage.

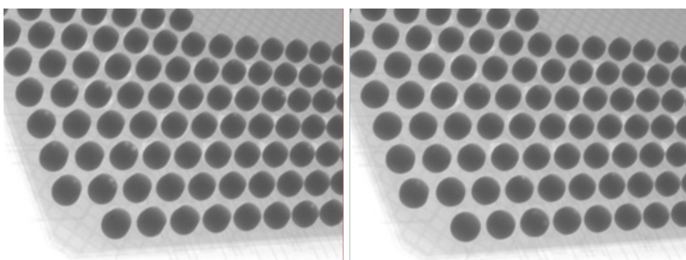

Figure 35: Left: DFLT, P210, PBVR = 0.5; Right: DFLT-2, P210, PBVR = 0.5.

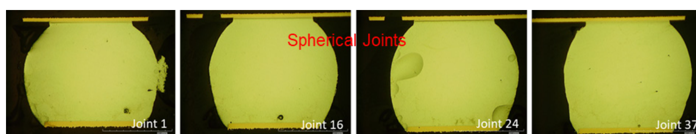

Figure 36: DFLT, P210 Joints, PBVR = 0.5.

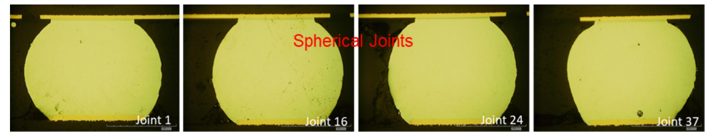

Figure 37: DFLT-2, P210 Joints, PBVR = 0.5.

Using an even hot profile of P220 and P240 but maintaining the PBVR of 0.13, both DFLT and DFLT-2 in Figure 38 had the ideal short-and-fat drum-shaped joints. The cross-sectional images in Figures 39, 40 and 41 confirm the desired drum joint shape for both the corner and middle joints. Middle joints are clearly taller than the corner joints for all three combinations, meaning the convex warpage of the assembly. P220 and P240 profiles on DFLT did not make the noticeable difference on the final joint shape, which is same in DFLT-2. No hot-tearing delamination or shrinkage voids were seen in any of the joints on the whole row.

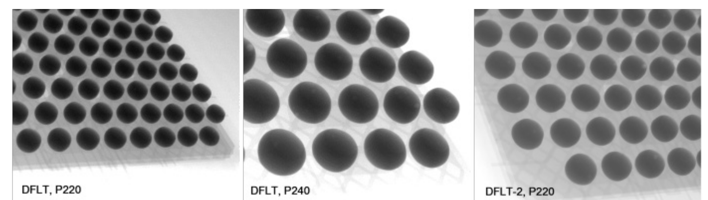

Figure 38: Left: DFLT, P220, PBVR = 0.13; Middle: DFLT, P240, PBVR = 0.13; Right: DFLT-2, P220, PBVR = 0.13.

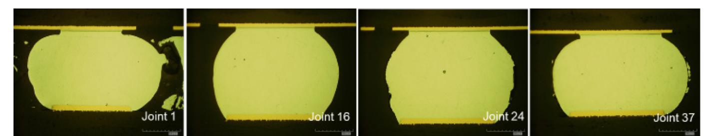

Figure 39: DFLT, P220, PBVR = 0.13. Left: the Corner Joint; Right: the Middle Joint.

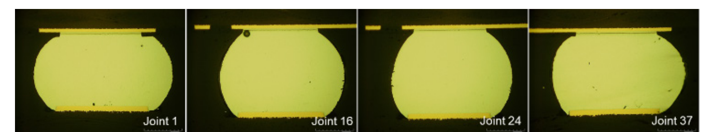

Figure 40: DFLT, P240, PBVR = 0.13. Left: the Corner Joint; Right: the Middle Joint.

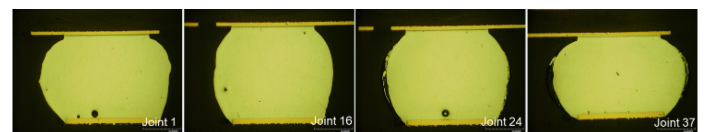

Figure 41: DFLT-2, P220, PBVR = 0.13. Left: the Corner Joint; Right, the Middle Joint.

In summary, BiSnAg has shown severe defects, including open joints, hot-tearing delamination, necking etc., under P185 profiles regardless of PBVRs. Increasing to reflow peak temperature by using P200 profile, BiSnAg joints have been dominated hot-tearing

and shrinkage voids.

Under P200 profile, DFLT and DFLT-2 can form the elongated joints under a PBVR of 0.5 without evident necking, while still presenting the partial hot-tearing open at one corner joint specifically for DFLT-2. Lower PBVR (0.13 and 0.25) tend to present more defects, including necking, hot-tearing delamination, and even HIP. With PBVR of 0.5, DFLT is presenting the acceptable joint morphology while DFLT-2 still have partial hot-tearing at one corner joint. Under P210 profile, both a PBVR of 0.25 and 0.5 led to the ovel shape or even spherical shape joints with no abnormal defects while PBVR of 0.13 still caused necking in the middle joints for both DFLT and DFLT-2.

Further increasing the reflow peak temperature to 220°C or higher, all three pastes formed the spherical shape joints in the middle and the drum shape joints at the corner and free of risky defects, as such necking, hot-tearing, HIP, NWO, and NCO etc.

Most of the packages assembled with BiSnAg paste had shown the concave warpage while both DFLT and DFLT-2 are prone to have convex warpage after reflowing. However, near-flat assemblies are still seen in a few processing combinations. Accidentally, the assembly reflowed with BiSnAg under P220 and PBVR=0.13 has shown the convex warpage, which is different from the other BiSnAg assemblies in Table 6. Similarly, DFLT-2, P200 and PBVR of 0.5 results in an assembly in concave warpage, different from the others. The warpage types of reflowed packages are summarized in Table 7, in which A represents convex warpage, B for concave warpage, C for flat or near-flat package and D for tilt assembly.

Table 7: The warpage type of reflowed assemblies.

Assembly Warpage	PBVR	Reflow				
		P185	P200	P210	P220	P240
BiSnAg	0.13	D	B		A	
	0.25	B	B			
	0.5	B	C		B	
DFLT	0.13		A	A	A	A
	0.25		C	A		
	0.5		C	A		
DFLT-2	0.13		A	A	A	
	0.25		C	A		
	0.5		B	A		

A: Convex; B: Concave; C: Flat; and D: Tilt.

DISCUSSION

Joint formation was influenced by the alloy selection, the reflow and PBVRs. To differentiate these impacts, the joint morphology was ranked based on the processing condition listed in Table 6. The joints were ranked into four levels based on the criteria shown in Table 8.

Table 8: Joint ranking criteria

Joint Score	Description
1	NCO/HIP/NWO/Hot-tearing/Bridging
2	Necking
3	Oval/Elongated
4	Spherical/Drum

The score of joints is then summarized in Table 9. All joints of ranking score of 1 are to be rejected due to the fatal defects. Necking joints (score 2) will not present immediate failure but bring the risk of failure near the necking area in service. Joints with scores of both 3 and 4 are acceptable with no processing concerns. The oval and elongated joints were formed under lower peak temperature (P200 and P210 profiles), which may indicate the formation of hybrid joint. The hybrid joints were formed when SAC305 ball did not fully melt or dissolve into LTS/MTS pastes during soldering and thus the joints were elongated and presented two distinct morphologies associated with SAC305 (package side) and LTS/MTS paste (PCB side) respectively. Hybrid joints may not bring the risk for long term reliability depending on the package design, the alloys of both ball and paste, and service conditions [18,19]. Using P210 profile and PBVR of 0.5, the spherical joints still present hybrid morphology through SEM observation [20]. The joints with drum shape reflowed under both P220 and P240 indicated the full melting and the thorough merging of both ball and paste during reflow and resulted in a uniform morphology [21].

Table 9: Joint Ranking Score

Joint Score	PBVR	Reflow				
		P185	P200	P210	P220	P240
BiSnAg	0.13	1	1		4	
	0.25	1	1			
	0.5	1	1		4	
DFLT	0.13		1	2	4	4
	0.25		2	3		
	0.5		3	4		
DFLT-2	0.13		1	2	4	
	0.25		1	3		
	0.5		1	4		

With the ranking scores in Table 9, a DOE analysis has been implemented to find the effective factors on joint morphology, shown in Figure 42. All three factors, including reflow, PBVR and alloy, have effective impacts on joint morphology. Reflow impact most while PBVR and alloy have similar effects, slightly above the threshold of 2.228. The impact from the combination of alloy and PBVR is slightly below the threshold value, indicating the inferior effect.

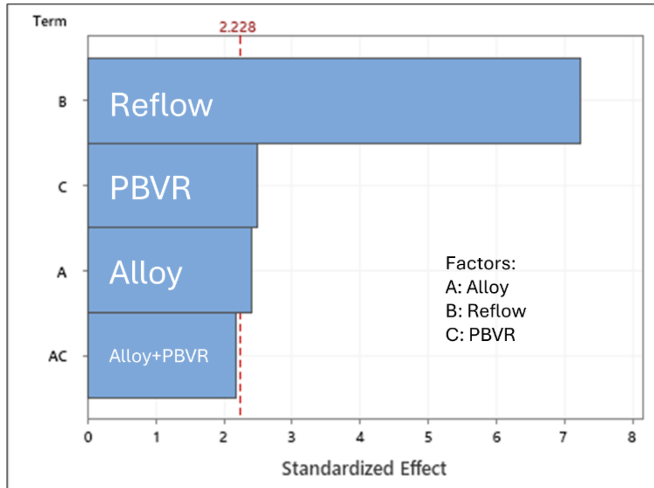

Figure 42: Response of Factors on Joint Morphology

In each factor term, the effects of selections were compared, seen in Figure 43. The hot profiles always deliver higher scores of joint morphologies, confirmed by P220 and P240 profiles with the spherical and drum shape joints regardless alloys and PBVR. In alloy selection, DFLT had the best score, DFLT-2 second, while BiSnAg ranked worst. PBVR improves joint morphology with increasing paste-to-ball volume ratio (more paste volume).

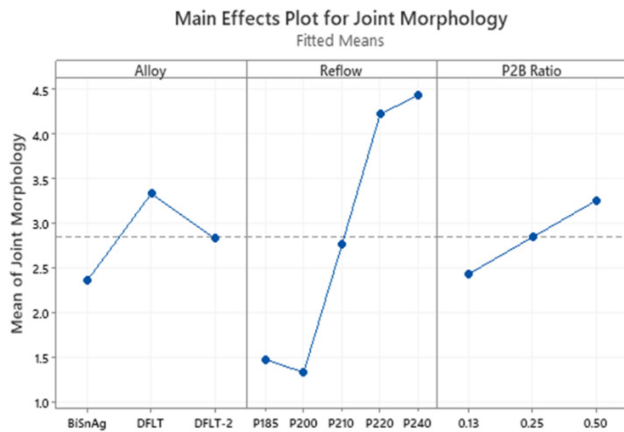

Figure 43: Main Effects of Factors on Joint Morphology

It is a surprise to see that hot profiles are more effective in reducing the defects caused by warpage of PBGA928, even larger convex warpage was presented under such hot profiles [22]. Near-flat assemblies are seen under P200 reflow for all three pastes, shown in Figure 15, 24, 25, and 27 and summarized in Table 7. However, if combining both Table 7 and 9 to check both assembly warpage and joint score, these four processing combinations lead to the poor joint scores although the package is flat or near-flat. Two (BiAgSn under P200 and PBVR of 0.5 in Figure 15 and DFLT-2 under P200 and PBVR of 0.25 in Figure 25) scored only 1 because of hot-tearing, one scored 2 (DFLT under P200 and PBVR of 0.25 in Figure 24) due to necking and one scored 3 (DFLT under P200 and PBVR of 0.5 in Figure 27) from an elongated joint shape. As a comparison, those assemblies reflow under hot profiles (P220 & P240) show the significant warpage while the joint morphology are still scored high for all three pastes even with PBVR of 0.13. This may indicate that the paste volume for PBGA928 reflow may not be a concern if reflow temperature is hot enough to melt both paste and SAC ball and provide sufficient molten solder to accommodate the warpage displacement during reflow.

Under the same processing condition of P200 and PBVR of 0.5, when joining with SAC305 ball, BiSnAg joints are dominated by hot-tearing defects while DFLT joints are dominated by elongated joints. Both joints are hybrid joints, in which pastes dominated the joint morphology at PCB side while SAC ball maintained the morphology at package side. Also, BiSnAg had a much larger hybrid zone than DFLT as shown in SEM images of Figure 44, which indicated that BiSnAg had more molten solder under P200 reflow than DFLT. However, severe hot-tearing in BiSnAg joints instead of DFLT joints may imply that alloy selection would be the key to reduce hot-tearing. Hot tearing in BiSnAg/SAC joints was attributed to the overlap of joint solidification temperature and inversion of package warpage [23]. If this is true, the thermal behavior of solder alloys will help to guide the selection of pastes.

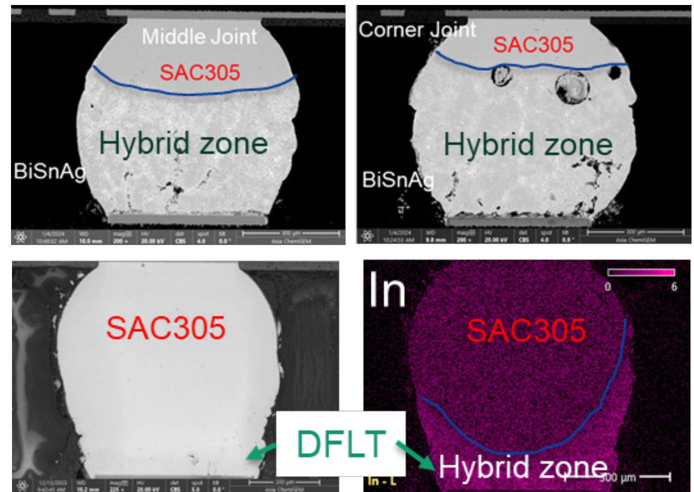

Figure 44: SEM images of BiSnAg/SAC joints (top) and SEM and EDX mapping images of DFLT/SAC joints (bottom) formed under P200 and PBVR of 0.5.

Figure 45 shows the binary phase diagram of Bi-Sn. When joining with SAC ball during reflow, BiSn eutectic solder melts first and dissolve SAC ball to move the molten alloy towards Sn-rich composition. The pasty range of the SAC305/BiAgSn joint increases with the increase of liquidus temperature and the constant eutectic solidus temperature till Sn content rising to 79wt%, and then the pasty range will decrease when solidus temperature starts to rise at a higher pace than the liqudus temperature. The maximum pasty range will be 58°C with the composition of 79Sn/21 Bi. Although the melting temperature is always around 139°C and above in BiSn system, the existence of undercooling will allow the

joint fully solidified below the melting temperature, which happen to overlap the solidification and the inversion of package warpage. This raises the risk of forming hot-tearing joints.

Different from BiSnAg, DFLT and DFLT-2 started with high Sn content in binary phase diagram of Figure 46. During reflow, the dissolution of Sn into DFLT and DFLT-2 continuously increases Sn content, which raises both solidus temperature and liquidus temperature, and reduces the pasty range. Solidus temperature of DFLT/SAC joint is much higher than the inversion temperature of 140°C. Even with significant undercooling, the joint may still likely be fully solidified above the inversion temperature of 140°C. This reduces dramatically the possibility of forming hot-tearing joints. DFLT-2 has around 10°C lower solidus temperature than DFLT, which may render a higher risk of forming hot-tearing joint. Compared to BiSnAg, both DFLT and DFLT-2 have much lower risk, which has been confirmed in current work.

Using higher reflow temperature to fully melt SAC and merge with BiSnAg will dilute Bi content dramatically and move joint composition to Sn-rich end. This will increase the solidus temperature exceeding 140°C when Bi is diluted to below 19wt% in final joints. This explains the healthy BiSnAg/SAC joints formed under hot P220 reflow, in which Bi content will be diluted to below 12wt% even with PBVR of 0.5 and it increases the solidification temperature in turn, which lowers the risk of hot-tearing.

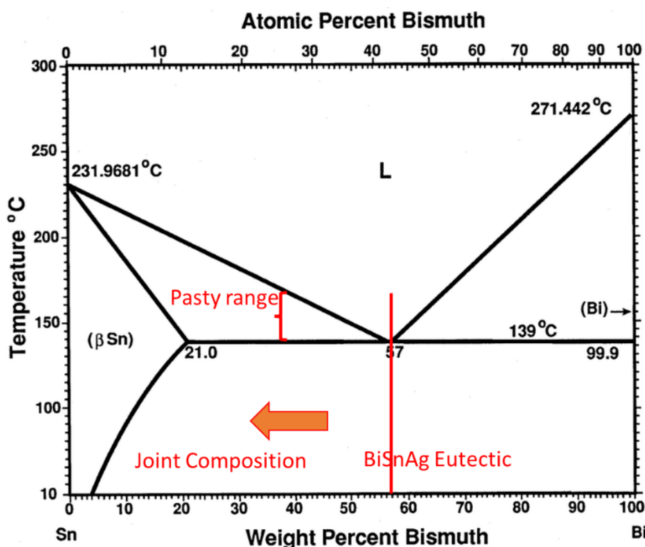

Figure 45: Binary Bi-Sn Phase Diagram and the Pasty Range with Composition.

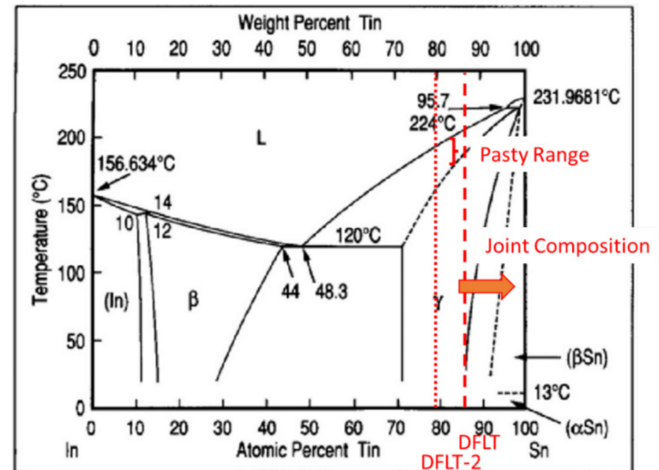

Figure 46: Binary In-Sn phase Diagram and the Pasty Range with Composition.

The warpage shape of reflowed package is associated with the solidification temperature as well. If joints were solidified decently above 140°C, the package would yield convex shape. Solidified below 140°C, concave shape will be seen. If the joints were solidified around 140°C, flat or near-flat package will be achieved. This explains that the concave warpage of most BiSnAg assemblies under P185 and P200 reflow, regardless of PBVR. It also accounts for the convex warpage of most DFLT and DFLT-2 assemblies reflowed under P210, P220 and P240 profiles.

In summary, it is still challenging to find an acceptable processing window for all three pastes to achieve the joints free of fatal defects under low temperature reflow of P185 and P200 (lower warpage). This is attributed to insufficient solder paste volume to accommodate the warpage displace of PBGA928. Adding more pastes helps to improve joint morphology but raises the risk of bridging. Increasing the reflow temperature to mid temperature regime (P210 and P220) or using traditional SAC305 profile of P240, the joints are formed better even though the reflowed packages are significantly warped. The hot profile will melt both paste and SAC ball and provide sufficient solder volume to accommodate the elevated warpage displacement. Under the threshold temperature reflow (P210), DFLT had improved joint morphology with increasing PBVR, which verifies the effectiveness of sufficient solder volume. The overlap of the joint pasty range and the warpage inversion brings the risk of hot-tearing and severe shrinkage voids. It is preferred to have the joint fully solidified before cooling down to the inversion temperature or joint solidification starts below inversion temperature. The warpage shape of reflowed package is determined by the relationship between joint solidification temperature and package inversion temperature.

So far, all the tests and observations are only based on PBGA928, whose maximum warpage may still be able to be handled by sufficient solder volume through higher temperature reflow and/or more paste volume. However, if the high temperature warpage is not able to be handled through reasonable solder volume, lower temperature soldering may become necessary to decrease the warpage. In that case, replacing SAC ball with lower melting solder

balls would lower the reflow temperature and help to provide sufficient solder volume and achieve healthy joints. The lower melting solder alloys, including SAC-Bi, SAC-In and even BiSn would possibly be used as potential alternatives [24, 25]. Preliminary studies, including joint formation under the combination of paste selections, reflow profiles and PBVRs as well as joint shear strength, have verified the success of lower temperature soldering by using both low temperature solder ball and solder paste. Partial work will be reported in Phase II.

CONCLUSIONS

The joint formation for PBGA928 surfaced with SAC305 balls has been studied under various soldering combinations. The challenges of low temperature soldering (P185 and P200) are seen for all three pastes regardless of PBVR. Mid temperature reflows (210°C and 220°C) improved the joint formation. 220°C peak temperature, allowing SAC305 to melt instead of dissolving, resulted in the formation of healthy joints for all three pastes even with PBVR of 0.13. The combination of 210°C peak temperature and PBVR of 0.5 can form the healthy joint for both DFLT and DFLT-2 pastes as well. Coincidence of joint solidification and warpage inversion would risk the joints with hot-tearing defects. Additional work is still ongoing to determine the specific plausible lower temperature processing window.

ACKNOWLEDGEMENTS

The authors would like to thank their colleagues, namely, Tyler Richmond, Kyle Aserian, Dominic Lu, Jie Geng, Yan Liu, Christine LaBarbera, Ian Tevis, Maria Htoo, Jasmine Wu, Haoxing You, Danyang Zheng and Mengyao Wen for the kind help.

REFERENCES

[1] P. Y. J. Su, et al., "Chiplets integrated solution with FO-EB package in HPC and networking application," in Proceedings of 2022 IEEE 72nd Electronic Components and Technology Conference (ECTC), 2022, pp. 2135-2140.

[2] C. L. Gan, & C. Y. Huang, Interconnect Reliability in Advanced Memory Device Packaging. Springer Nature, 2023

[3] L. Sun, et al., "A new low-temperature solder assembly technique to replace eutectic Sn-Bi solder assembly," Micromachines 13.6, 2022, pp. 867.

[4] J. H. Wong, et al., "Warpage and RDL stress analysis in large fan-out package with multi-chiplet integration," in Proceedings of the 2022 IEEE 72nd Electronic Components and Technology Conference (ECTC), 2023, pp. 1074-1079.

[5] R. N. Das, et al., "Extremely Large Area Integrated Circuit (ELAIC): An Advanced Packaging Solution for Chiplets," in Proceedings of the 2023 IEEE 73rd Electronic Components and Technology Conference (ECTC), 2023, pp. 258- 265.

[6] G. Xu, et al., "Simulation and experiment on warpage of heterogeneous integrated fan-out panel level package," in Proceedings of the 2021 IEEE 71st Electronic Components and Technology Conference (ECTC), 2021, pp. 1044-1049.

[7] D. S. Lai, et al., "Better Warpage Control by Using Low Temperature Solder for Large FCBGA Application," in Proceedings of the 2021 International Conference on Electronics Packaging (ICEP), 2021, pp. 135- 136.

[8] J. Lau, "Recent advances and trends in advanced packaging," IEEE Transactions on Components, Packaging and Manufacturing Technology, vol. 12, no. 2, 2022, pp. 228-252.

[9] P. Su, et al., "Design-for-Manufacturing and Design-for-Reliability Strategies for Large 80mm+ 2.5D Devices," in Proceedings of the 2023 IEEE 73rd Electronic Components and Technology Conference (ECTC), 2023, pp. 706- 712.

[10] H. Fu, et al., "INEMI Project on Process Development of BiSn-Based Low Temperature Solder Pastes," in Proceedings of SMTA International 2017, 2017, pp. 207- 220.

[11] H. Fu, et al., "INEMI Project on Process Development of BiSn-Based Low Temperature Solder Pastes, Part IV: Comprehensive Mechanical Shock Tests on POP Components Having Mixed BGA BiSn-SAC Solder Joints," in Proceedings of SMTA International 2018, 2018, paper LF1_P1.

[12] H. Fu, et al., "INEMI Project on Process Development of BiSn-Based Low Temperature Solder Pastes, Part VI: Mechanical Shock Results on Resin Reinforced Mixed SnAgCu-BiSn Solder Joints of FCBGA Components," in Proceedings of SMTA International 2019, 2019, pp. 513- 525.

[13] R. Coyle, et al., "Interim Thermal Cycling Report on Hybrid, Homogeneous, and Resin Reinforced Low Temperature Solder Joints," in Proceedings of SMTA International 2021, 2021, pp. 401- 426.

[14] K. K. Tang, "LTS Manufacturing Challenges and Solutions," in INEMI Low Temperature Soldering Workshop, Apr. 24, 2019.

[15] W. Shen, "Effect of warpage on solder joint fatigue life by influencing the solder joint shape in BGA packages," IEEE Transactions on Components, Packaging and Manufacturing Technology, vol. 14, no. 4, 2024, pp. 611-618.

[16] W. K. Loh, et al., "Impact of low temperature solder on electronic package dynamic warpage behavior and requirement," in Proceedings of 2019 IEEE 69th Electronic Components and Technology Conference (ECTC), 2019, pp. 318- 324.

[17] "Coplanarity Test for Surface-Mount Semiconductor Devices", JESD22-B108B Jedec Standard, September 2010.

[18] R. Coyle, et al., "Thermal Cycling Hybrid, Homogeneous, and Resin Reinforced Low Temperature Solder Ball Grid Array Interconnects at a High Homologous Temperature," in Proceedings of SMTA International 2024, 2024, pp. 223- 239.

[19] F. Mutuku, et al., "A Near-Eutectic Sn-Bi Low-Temperature Alloy with High Thermal Fatigue Resistance," in Proceedings of SMTA International 2023, 2023, pp. 345- 352.

[20] H. Zhang, et al., "The attempt of lower temperature soldering for large plastic ball-grid array board level assembly," in Proceedings of IPC APEX EXPO 2024 ECWC16, Session 20, 2024.

[21] F. Mutuku, et al., "Effects of Dynamic Warpage on Solder Joints of Large Plastic Ball-Grid Arrays Assembled with LTS," in Proceedings of SMTA International 2024, 2024, pp. 285- 290.

[22] W. K. Loh, et al., "Recent trend of package warpage characteristic.," in Proceedings of 2015 International Conference on Electronics Packaging and iMAPS All Asia Conference (ICEP-IAAC), IEEE, 2015, pp. 233- 238.

[23] H. Fu, et al., "INEMI Project on Process Development of BiSn-Based Low Temperature Solder Pastes," in Proceedings of SMTA International 2017, 2017, pp. 207.

[24] N. B. Jaafar, et al., "Comprehensive Study on Thermal Aging and Ball Shear Characterization of SAC-X Solders," in Proceedings of 2021 IEEE 23rd Electronics Packaging Technology Conference (EPTC), 2021, pp. 430- 434.

[25] M. Koide, et al., "Full Low Temperature Solder BGA Development for Large size BGA Package," in Proceedings of 2020 IEEE 70th Electronic Components and Technology Conference (ECTC), 2020, pp. 1265- 1269.

BIOGRAPHIES

Dr. Hongwen Zhang is the Principal Research Metallurgist and Senior R&D Manager in Indium Corporation. He has been working on the development of lead-free solder materials for more seventeen years. He holds a Doctorate in Materials Science & Engineering and Masters from both Materials Science & Engineering and Mechanical Engineering. He leaded the invention of the Durafuse® technology, and had been granted more than twenty patents globally. He is a certified SMT Process Engineer and certified specialist for IPC-A-600 and IPC-A-610D. He had been awarded as 2023 SMTAi Member of the Technical Distinction.

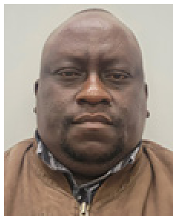

Francis M. Mutuku is a Senior Research Metallurgist in the Department of Research and Development at Indium Corporation. He has 7+ years of experience in Pb-free solder materials design and development, processing optimization and the associated technologies for low temperature, mid-temperature and high-reliability applications. He has co-authored more than 35 conference papers and several journal papers. He interfaces with customers to offer solutions to various emerging issues for existing and new products. Francis M. Mutuku has a Ph.D. in Physics (Materials) from SUNY Binghamton University, a Bachelor's of Science (Physics) from Egerton University in Kenya, Post Graduate Diploma in Education (PGDE) from Egerton University in Kenya and a Certified SMT Process Engineer (CSMTPE).

Dr. Huaguang Wang is a Research Metallurgist in the Research & Development Department at Indium Corporation. His work focuses on the development of low- and mid-temperature, lead-free solder materials with high reliability. Dr. Wang has coauthored numerous technical papers and holds several patents in the field of lead-free solder innovation. He earned his Ph.D. in Materials Science and Engineering from Michigan Technological University, and holds both a master's and a bachelor's degree in Metallurgical Engineering from Central South University in China. He is also a Certified SMT Process Engineer.